Available online at www.sciencedirect.com

SciVerse ScienceDirect

Ceramics International 38 (2012) 1447–1462

CERAMICS INTERNATIONAL

www.elsevier.com/locate/ceramint

Steel ladle well block *post mortem* analysis

M.A.L. Braulio [a,*], E.W. Zinngrebe [b], S.R. van der Laan [b], V.C. Pandolfelli [a]

[a] *Federal University of São Carlos, Materials Engineering Department, FIRE Associate Laboratory, São Carlos, SP 13656 905, Brazil*
[b] *Tata Steel RD&T, Ceramics Research Centre, The Netherlands*

Received 14 January 2011; received in revised form 7 September 2011; accepted 9 September 2011
Available online 16 September 2011

Abstract

Spinel-containing castables are widely used as steel ladle refractory lining, due to their outstanding basic slag (calcium aluminate based) corrosion resistance. In order to understand their corrosion mechanism, a *post mortem* evaluation of a steel ladle well-block castable was carried out. The interaction among the refractory castable, slag and molten steel was mainly evaluated by light optical and scanning electron microscopy using SEM multielement mapping. The results indicated that an equilibrium state was attained, leading to the formation of a densified barrier that protected the original castable from corrosion located at the deepest regions, regarding the metal flow. Each one of these layers was evaluated, underscoring the damage that the refractory is liable to during application and also the possibilities of steel contamination, due to castable wear, and reoxidation. The experimental results were compatible with the literature, pointing out how corrosion takes place and the possibilities to reduce its negative effect.

Keywords: C. Corrosion; D. Spinels; E. Refractories

1. Introduction

Steel ladle refractory lining wear is usually associated with slag dissolution and is often speeded up by spalling. During molten steel treatment, the refractory can be impregnated and thus deteriorate due to various mechanisms, such as temperature-induced phase transformation and thermomechanical property change throughout the temperature profile. Consequently, cracking takes place parallel to the material's hot face, leading to lining spalling [1]. According to Mattilla et al. [2], chemical wearing usually causes degradation in the refractories, followed by thermal and mechanical wearing.

Lee and Zhang [3] stated that refractory microstructures (i.e., composition, texture and distribution of grain and matrix phases), bath and slag properties (mainly composition and viscosity as a function of temperature) and their wetting and interaction at high temperatures should be evaluated together in order to understand the corrosion mechanisms properly. In their review of melt corrosion of refractories, these authors also pointed out that the refractory and liquid in contact should form a near-equilibrium system in order to limit the extent of dissolution of the refractory into the slag and that the crystal structure of magnesium aluminate spinel ($MgAl_2O_4$) enables it to pick up cation impurities from the liquid. Considering these aspects, alumina–magnesia refractories have been widely used in steel ladles and, in particular, as precast castable blocks [4,5].

In this context, various studies were carried out to elucidate the benefits of adding spinel to refractories, aiming to withstand the corrosion by basic slag. Sarpoolaky et al. [6] analyzed the influence of the aggregate source (white-fused alumina, tabular alumina, brown-fused alumina and alumina-rich spinel) on slag corrosion of low-cement containing castables. In their study, the attack of the bond system is reported to occur firstly between the slag liquid (high CaO, MnO and FeO contents) and the calcium aluminates and alumina of the matrix. Thus, the local liquid (predominantly $CaO–Al_2O_3–SiO_2$) contained a higher amount of CaO that could react with the matrix and aggregates, usually leading to CA_6 formation. Comparing the compositions with different aggregates, white-fused and tabular alumina showed extensive penetration, although the corrosion was lower. For brown-fused alumina, titanate phases of the aggregate resulted in high refractory densification, reducing the liquid penetration. Nevertheless, a large volume of fluid liquid was generated and, thus, corrosive wear was extensive.

* Corresponding author.
E-mail address: mariana.gemm@gmail.com (M.A.L. Braulio).

0272-8842/$36.00
doi:10.1016/j.ceramint.2011.09.027

Conversely, spinel grains led to low penetration and corrosion and are recommended for application to refractory castables.

Zhang et al. [7] compared the corrosion of alumina grains (white-fused and tabular) by FeO and MnO-containing CMAS ($CaO–MgO–Al_2O_3–SiO_2$) slag and detected the formation of CA_6 and hercynitic spinel ($FeO·Al_2O_3$) layers at the alumina-slag interfaces. For tabular alumina, these layers were incomplete, resulting in a direct attack of slag via pores and grain boundaries. In parallel, Vázquez et al. [8] evaluated the corrosion of polycrystalline corundum and calcium hexaluminate by calcium silicate slag, pointing out a homogeneous reaction front for alumina, whereas hibonite (CA_6) led to an irregular reaction front. This feature was attributed to the crystal habit of CA_6 and its lower densification during sintering, resulting in an open microstructure that could be easily penetrated by slag, through porosity and grain boundaries. These authors also stated that the capillary movement of liquid phase among the CA_6 grains would result in an area of high densification, reducing the overall porosity and then increasing the corrosion resistance.

Another aspect that affects the corrosion of this system is the composition of the magnesium aluminate spinel. Whereas alumina-rich spinels (90 wt% of Al_2O_3) dissolve indirectly due to the free alumina available and their ability to form spinel and CA_6 at the grain/slag interfaces, near stoichiometric spinels (78 wt% Al_2O_3) present direct dissolution. As a consequence of the greater amount of Mg^{2+} vacancies for the alumina-rich spinels, more cations from the slag can be accommodated and then the local liquid becomes silica-rich, increasing its viscosity and reducing the penetration. On the other hand, thermodynamic calculations showed better corrosion resistance of the near stoichiometric spinel as more slag is required to fully dissolve it [9].

Furthermore, the content of synthetic spinel ($MgAl_2O_4$) or magnesia (that results in the *in situ* spinel formation at temperatures above 1200 °C for high-alumina containing castables) [10] is an important selection variable for the corrosion and penetration behavior of the refractory. A greater amount of synthetic spinel or MgO leads to a slight increase in corrosion, but a reduction in the penetration by the molten slag [11]. According to previous work [12], spinel amount close to 20 wt% would optimize both requirements. Below the optimum amount, the corrosion resistance is spoiled, due to a lack of proper spinel content, whereas above 20 wt% it leads to the reduction of the slag infiltration resistance.

The spinel grain size also influences the slag penetration and corrosion resistance. The use of fine grains leads to greater effectiveness, as a result of their better distribution throughout the castables matrix. Nevertheless, they could also lead to high sinterability and, thus, shrinking cracks, lowering the infiltration resistance [13]. Additionally, the corrosion degree of synthetic spinel containing castables is usually higher than the one attained for *in situ* spinel-forming castables [14]. As this reaction is followed by expansion [10], extensive shrinkage can be avoided. Conversely, extensive expansion can lead to cracks and reduces the infiltration resistance. Therefore, the expansion of this system must be designed, in order to attain a suitable balance between sintering and expansion.

Considering that almost all the work in the literature was carried out in the laboratory, taking into account only a single working cycle and just chemical aspects (but not the thermo-mechanical ones), studies that could show more realistic aspects are still required. In this context, this work addressed the *post mortem* evaluation of a used alumina-spinel well block at Corus–IJmuiden steel shop (The Netherlands) in order to highlight two main features: (i) how to ensure clean steel production and avoid its reoxidation and (ii) to understand how the refractory castables perform and figure out how the interaction between the refractory and the melt could be minimized. Although the well block is a comparatively small refractory part in the ladle, it is located at a crucial spot (ladle outlet) and, thus, can affect the steel quality. It is also subjected to harsh conditions, including thermal shock, contact with steel and slag, and creep. Fig. 1 indicates the location of the well block in the ladle design.

2. Materials and techniques

Concerning the steel-ladle processing parameters at Corus–IJmuiden steel shop, almost all of its melts are Al killed and its average life is about 85 heats for the bottom and, thus, also for the well block. For the evaluated well block, the wrecking took place earlier at 64 heats, due to damage in the upper part of the ladle. The steel temperature during casting was in the range of 1550–1570 °C, whereas the temperature at tapping from the converter was considerably higher (between 1600 and

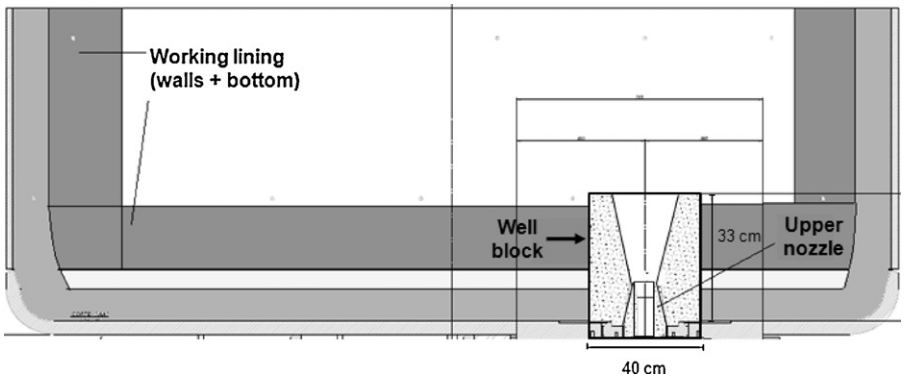

Fig. 1. Well block location at the bottom of the steel ladle.

1700 °C). Nevertheless, during tapping, transport and ladle treatment (except for ladle furnace), the steel temperature decreases to roughly 1560 °C during casting.

Following the end of casting, the ladle is firstly tipped, in order to take out the slag and then tilted 90°, when the nozzle is cleaned with oxygen lance and the sliding gates are replaced, if necessary. Additionally, the ladle slag line is mechanically cleaned. The ladle bottom is only cleaned if large pieces of slag were left behind after tipping the slag. As the upper nozzle is cleaned with oxygen lance, the iron oxide that is formed while cleaning the nozzle runs down into the ladle, on the well block. Therefore, the well block is also subjected to chemical attack by liquid iron oxide. Regarding the ladle glaze/slag, it is not removed from the well block, unless a big lump of it is formed.

After cleaning, the ladle is put upright again and the well filler (roughly 40 kg of chromite and quartz sand) is charged into the nozzle and well. Thus, in principle, the well block is covered with well filler during converter tapping. Further additions during tapping are always carried out into the tapping stream and, therefore, do not have contact with the well block, as the tapping impact area is opposite from the well block area. Following the well filler charging, the ladle is only left to cool in air, if it is expected to be used again quickly. Otherwise, it is either covered with a lid or it is moved to a heating stand, where a gas burner keeps its temperature close to 1000 °C. The empty time between the different heats is usually 30 min, at least, as the ladle is transported from the caster, tipped, cleaned, prepared and then transported again. Taking into account the processing environment and the conditions of the well block sampling, its evaluation could provide feedback on how to improve the well block performance, ensuring clean steel production.

Table 1 shows a typical slag chemical composition range of the ladle slag which has been killed after tapping, pointing out that it is basically a calcium aluminate slag, containing small amounts of MgO, SiO_2, TiO_2, MnO, FeO/Fe_2O_3.

The well block refractory castable evaluated in this study is a synthesized spinel-containing material bonded with calcium aluminate cement (RHI, Austria). Table 2 indicates the chemical analysis of this castable and some of its physical properties. Further information of this material will be provided in the next section. Additional tests carried out for this castable were the assisted sintering (thermal expansion) and the creep test, both performed in refractoriness-under-load equipment (Model RUL 421E, Netzsch, Germany). From the assisted sintering technique, the expansion behavior was analyzed and the expansive phases of the system were determined [10]. Cylindrical samples (50 mm × 50 mm) were prepared according to the 51053 DIN standard, cured at 50 °C and dried at 110 °C for one day, followed by pre-firing at 600 °C for 5 h before testing. For this evaluation, samples were heated up to 1500 °C (3 °C/min) and kept at this temperature for 5 h. The compression load applied was 0.02 MPa. The creep test was also performed, but in samples previously fired at 1550 °C for 24 h in order to avoid deformation due to sintering. The creep measurements were carried out at 1450 °C for 24 h under a constant compression load of 0.2 MPa.

Table 2
Chemical analysis and physical properties of the well block composition.

Chemical analysis	
Oxide	Amount (wt%)
Al_2O_3	89
CaO	2.3
SiO_2	0.1
MgO	8.1
Physical properties	
Apparent porosity (as-received)	17%
Apparent porosity (1500 °C × 4 h)	21%
Permanent linear change (1500 °C × 4 h)	0.2%
RUL–0.2 MPa ($T_{0.5}$)	1594 °C

Microstructure analyses were conducted at two different stages: (i) before the castable was applied to the steel ladle and (ii) for a well block sample collected after 64 heats in the ladle. For the castable evaluation before using, XRD quantitative analysis (TOPAS 4.1, Bruker, Germany) of a sample fired at 1500 °C for 5 h and scanning electron microscopy (JEOL JSM - 5900 LV, Japan) before and after this firing were carried out. The well block sample collected after the use (ii) is shown in Fig. 2 and a polished mount of a throughcut of the encrusted slag and cracked surface was prepared from it (5 cm × 3 cm). The throughcut was studied using light microscopical techniques (Zeiss Z1 Imager petrographical microscope using reflected light) as well as by SEM. Local bulk and phase compositional evaluation was carried out using SEM multielement mapping (spectral imaging, Thermo Noran NSS 2.2 analyzer).

3. Results

3.1. Well block castable characterization (before using)

A previous characterization of the well block was carried out before the *post mortem* evaluation. Goto et al. [15] pointed out the importance of this initial microstructure analysis to provide some general information related to the corrosion/infiltration behavior of the refractory. Fig. 3 shows the results of the assisted sintering technique (linear expansion and its derivative) for this castable (well block–WB), compared with two

Table 1
Chemical composition of killed ladle slag after tapping.

	Oxide content (wt%)						
	Al_2O_3	MgO	CaO	SiO_2	TiO_2	MnO	FeO/Fe_2O_3
Average	31.8	3.3	48.3	5.7	0.5	2.4	5.2
Standard deviation	5.9	0.8	4.1	2.2	0.2	0.8	2.4

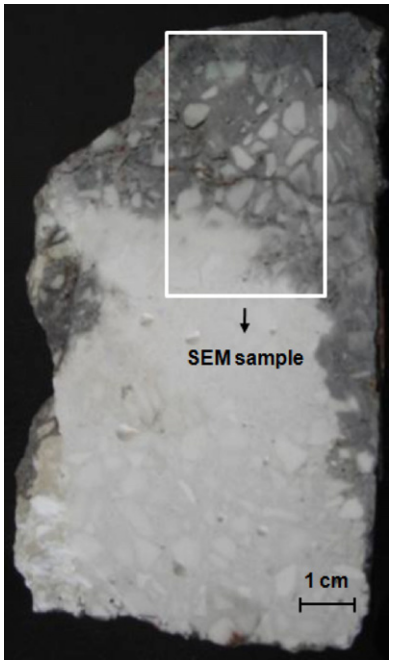

Fig. 2. Well block collected sample after 64 ladle heats, highlighting the area selected for SEM evaluation.

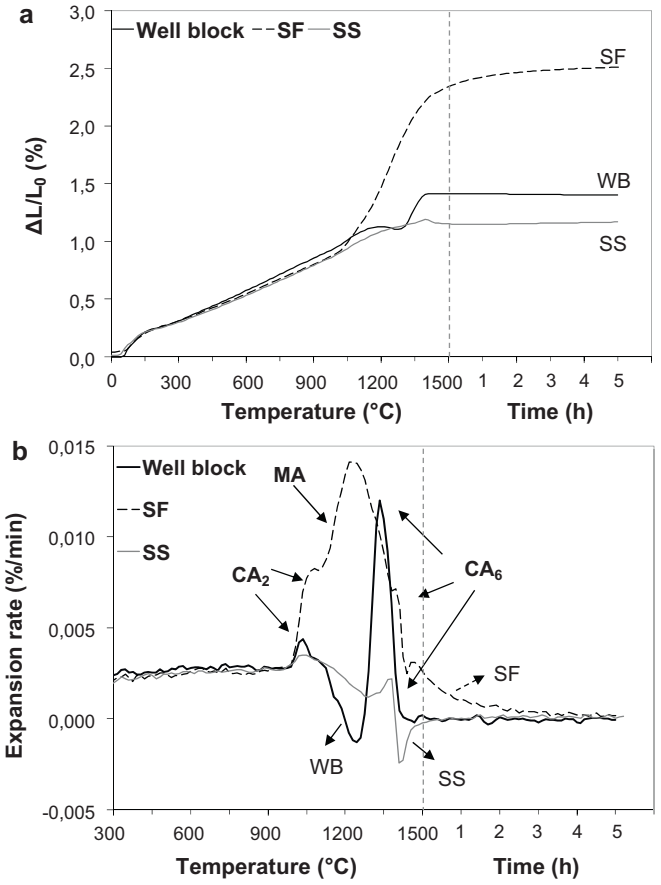

Fig. 3. (a) Expansion curves and (b) expansion rate up to 1500 °C (dwell of 5 h) of the well block (WB), *in situ* spinel-forming (SF) or synthetic spinel-containing (SS) castables. CA_2: calcium dialuminate; MA: magnesium aluminate spinel ($MgAl_2O_4$); CA_6: calcium hexaluminate.

references (*in situ* spinel-forming castable–SF and synthetic spinel-containing castable–SS, both bonded with 6 wt% of calcium aluminate cement without any microsilica addition) [16,17]. Although the chemical analysis (Table 2) indicated roughly 8 wt% of MgO, the expansion level observed was considerably lower than the one observed for the *in situ* spinel-forming castable, consistent with the presence of synthetic spinel in the well block composition instead of free magnesia. The derivative of the expansion curves (expansion rate) showed two peaks related to the calcium aluminate phase formation (CA_2 and CA_6), as previously stated in the literature [16] and similar to those for the synthetic spinel-containing composition (SS). Nevertheless, the expansion levels between the well block castable and SS were distinct and the calcium aluminate phase expansion peaks showed different intensities, which can be mainly a consequence of different calcium aluminate cement content, distinct apparent porosity and pore distribution, and also different sources of calcined and reactive aluminas [17] (unknown for the well block composition).

In Fig. 4, the microstructure evaluation of the as-received well block castable (a) and after its firing at 1500 °C for 5 h (b) indicates that it comprises synthetic spinel (MA–75 wt% Al_2O_3 and 25 wt% MgO) and tabular alumina as aggregates and it is a

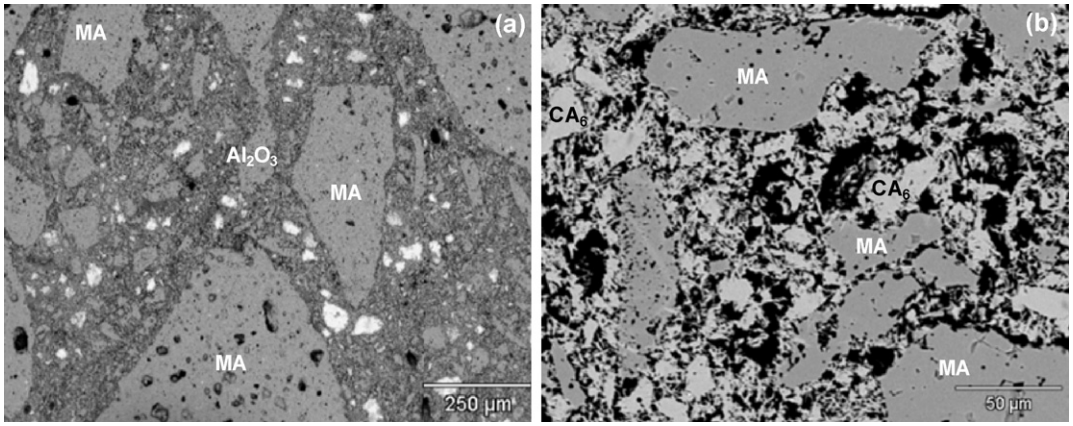

Fig. 4. Microstructure evaluation of (a) the as-received well block castable (the white phases are calcium aluminates, CA and CA_2) and (b) after its firing for 5 h at 1500 °C. MA: magnesium aluminate spinel ($MgAl_2O_4$); CA_6: calcium hexaluminate.

cement bonded refractory castable. The as-received composition microstructure implied that it was previously fired at temperatures in the range of 1000–1200 °C [18], as it did not show any cement hydrates, but calcium aluminates (CA and CA_2). After firing at 1500 °C, all these calcium aluminates reacted with alumina to form calcium hexaluminate (CA_6). The quantitative XRD analyses indicated that this castable fired at 1500 °C contains approximately 40 wt% of Al_2O_3, 25 wt% of $MgAl_2O_4$ and 26 wt% of CA_6. If the cement added to the composition was the most usual one applied for this sort of castable (70 wt% Al_2O_3–30 wt% CaO) [19], the XRD estimated CA_6 content and the castable chemical composition show an initial addition in the range of 7–8 wt% of calcium aluminate cement.

Thus, this fired castable is CA_6-bonded containing Al_2O_3 and $MgAl_2O_4$ as aggregates. Such refractory design is consistent with the work presented by Sarpoolaky et al. [6]. Nevertheless, this castable does not show the *in situ* spinel formation, which is well known to increase the corrosion resistance of steel ladle lining materials [20,21]. Furthermore, the well block castable did not contain fumed silica in its composition, and its absence can ensure better hot chemical and mechanical properties, such as creep and corrosion resistance, as well as hot modulus of rupture [22,23]. The lower creep linear deformation (Fig. 5), after 24 h at 1450 °C under a load of 0.2 MPa is in accordance with this assessment, as the addition of fume silica (1 wt%) in the SF castable reference resulted in high creep deformation.

3.2. Well block sample overview (after using)

The bright and dark field optical light images of the selected well block SEM sample (Fig. 2) is shown in Fig. 6. Whereas Fig. 6a shows the different reacted zones, as well as cracks, densification and iron droplets, Fig. 6b points out the sample's darkening, which is associated with the FeO/MnO infiltration in the slag system.

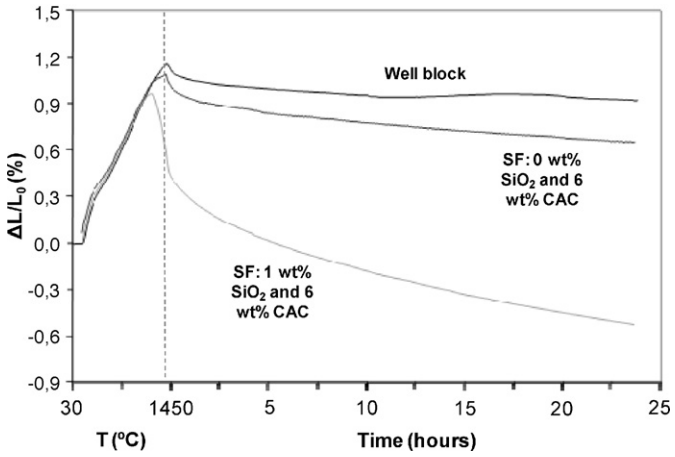

Fig. 5. Creep resistance (1450 °C × 24 h, 0.2 MPa) for the well block composition, compared with spinel-forming (SF) castables containing 6 wt% of calcium aluminate cement (CAC), with (1 wt%) or without (0 wt%) microsilica (SiO_2).

As can be detected in Figs. 2 and 6, the *post mortem* well block surface shows a distinct sequence of layers parallel to the surface, in contact to molten metal and slag. These layers are highlighted in Fig. 6a and numbered (i) to (v), ranging from the apparently unchanged inner part of the sample towards the outer corroded surface. The characteristics of these layers are as follows:

(i) Uncorroded refractory castable;
(ii) Densified region;
(iii) Thick layer comprising a homogeneous phase assemblage and also cracks (sometimes infiltrated by steel droplets);
(iv) Extended wearing region;
(v) Top layer comprising heterogeneous patches of slag.

3.3. Description of zones in the post mortem well block sample surface

3.3.1. Zone (i): uncorroded refractory castable

The microstructure of the first zone (deepest zone preserved in the sample) is similar to that shown by the well block refractory castable fired at 1500 °C (Fig. 4b), comprising magnesium aluminate spinel and alumina as aggregates, bonded with a matrix containing mostly CA_6. This aspect points out that this region was subjected to temperatures above 1500 °C, as its microstructure was similar to the one presented

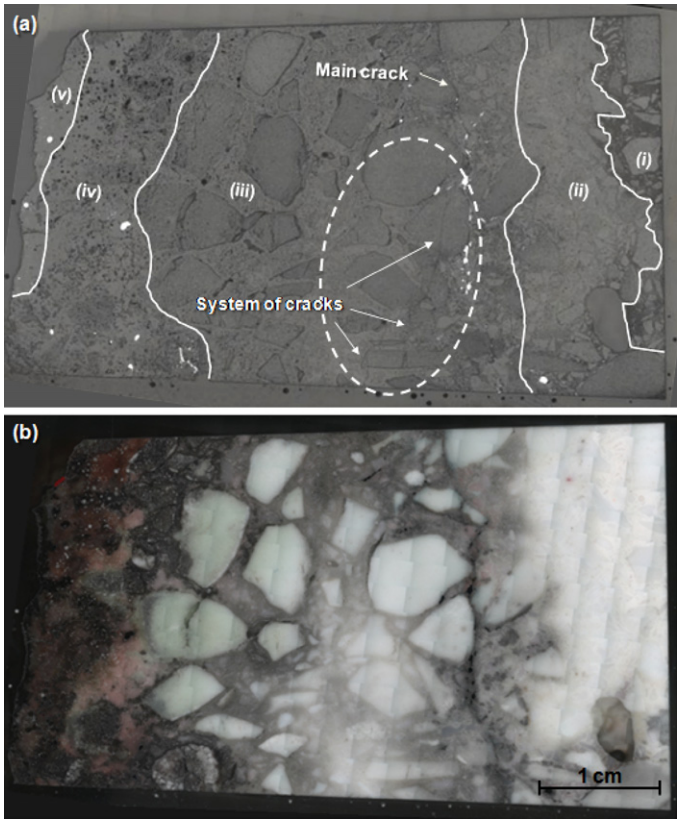

Fig. 6. (a) Brightfield and (b) darkfield optical light images of the used well block sample. In the brightfield image (a), cracks, iron (white droplets) and densification were detected. The different reacted zones (i–iv) are identified. The darkfield image (b) points out the sample's darkening, related to the FeO/MnO infiltration.

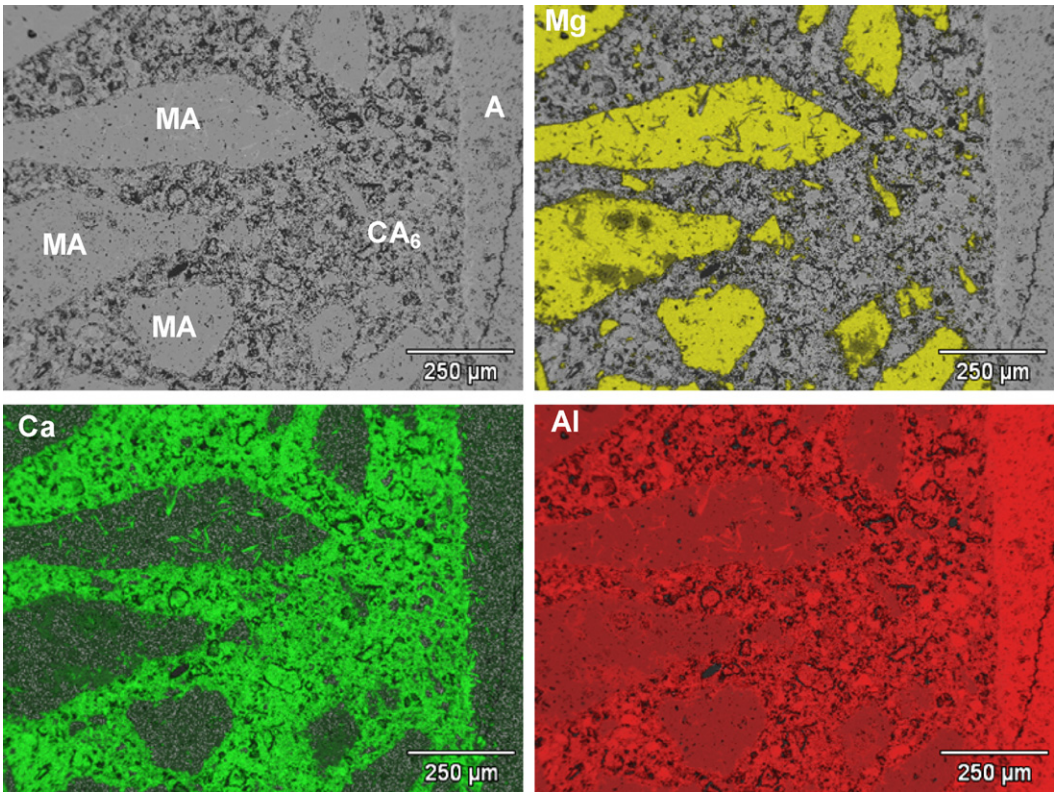

Fig. 7. Chemical mapping indicating the distribution of magnesium (Mg), calcium (Ca) and aluminum (Al) in a representative area of zone (i).

in Fig. 4b. A chemical mapping of a representative area of this zone is given in Fig. 7. This region attained temperatures high enough to lead to the CA_6 forming reactions and the associated sintering, but it was not subjected to any influence of external reactants or loss of matter to the outside of the castable. This is also supported by the absence of SiO_2 in this region (not found by EDX), showing the lack of infiltration of any external slag which would have carried silica with it.

Table 3 presents the bulk chemical composition of the castable's matrix in zone (i), as calculated from integration over selected areas in Fig. 7. This table also shows the bulk chemical composition of the densified region (zone (ii)), as will be mentioned below. The small amount of MgO indicates that a low content of finer spinel grains were also spread throughout the matrix. Additionally, from the image (Fig. 7, BSE grey image) the matrix porosity is estimated to be 36 vol% based on the segmentation of the dark areas.

3.4. Zone (ii): densified layer

Zone (ii) is the first visibly altered region of the wear profile of the well block (Fig. 6). It follows in a depth of 4 cm below the remaining surface and is formed from the underlying apparently unchanged refractory along a sharp termination front visible in Fig. 6. Microstructurally, the main feature of this layer is the strongly densified matrix among the aggregate grain shapes (Fig. 8).

In zone (ii), aggregates and the matrix can still be clearly separated. However, both have extensively recrystallized. The borders between aggregate grains and matrix are locally unsharp because of crystal new growth across them. The

Table 3
Castable matrix chemical composition in zone (i) and in zone (ii).

Oxides	Content (wt%)				
	Al_2O_3	MgO	CaO	SiO_2	Na_2O
Zone (i)	92.4	0.6	6.8	–	0.1
Zone (ii)	72.6	1.2	12.2	13.9	0.1

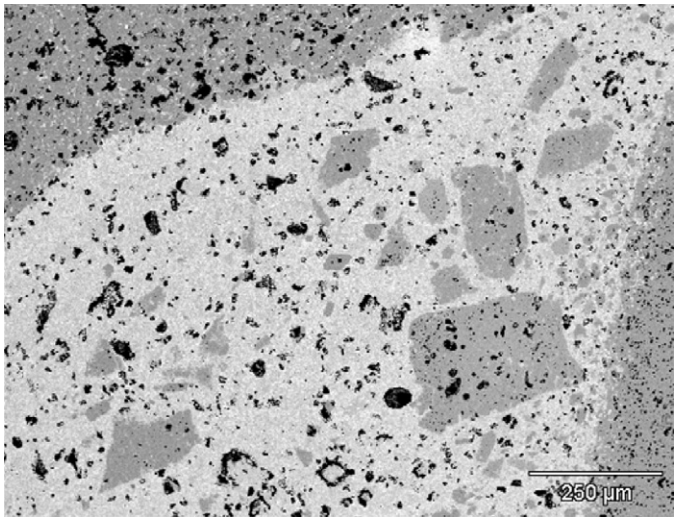

Fig. 8. SEM image of the densified layer–zone (ii). The tiny white areas between the CA_6 in the matrix indicates the location of an intercrystalline liquid.

crystallite size in both aggregates and matrix is consistently small, in the order of 10 μm or less. Aggregates consist of a dense intergrowth of alumina or spinel crystallites with interspersed CA_6 tablets. The matrix comprises a dense mass of CA_6 crystals bound by an intergranular silicate glass. The porosity in the matrix was strongly reduced compared to the unchanged refractory and is estimated to be ca. 9–10 vol% based on a grey-level segmentation in Fig. 9. Individual micropores, which are overwhelmingly closed, tend towards more rounded bubble like shapes than micropores in the unchanged matrix (zone (i)).

A representative chemical mapping of aggregates and matrix in this densified layer (ii) is shown in Fig. 9. The main characteristic of this region is its high silica content, which sharply contrasts to the original matrix (SiO_2-free).

According to the chemical mapping, recrystallization of the aggregates is accompanied by infiltration of elements into the aggregates, such as Ca and Si into alumina aggregates, mostly by liquid infiltration. Spinel aggregates were much more strongly affected by chemical alteration than the alumina ones, indicating significant CA_6 formation inside the spinel aggregates as well as silicate liquid infiltration. The matrix itself was turned into a roughly homogeneous assemblage of CA_6 plus liquid silicate and MgO was evenly distributed as a component. This liquid shows a slight tendency to concentrate along both spinel and alumina aggregate outlines, as seen in the element map for Si in Fig. 9.

The local bulk composition for the matrix in the densified zone (ii) has been measured by the extended area EDX in representative regions of the matrix depicted in Fig. 9, helped by the very fine grained and homogeneous state of the matrix (Table 3). Essentially, the matrix composition of the densified zone (ii) is comprised within the CMAS ($CaO–MgO–Al_2O_3–SiO_2$) system and has a remarkably high SiO_2 content. Na_2O is

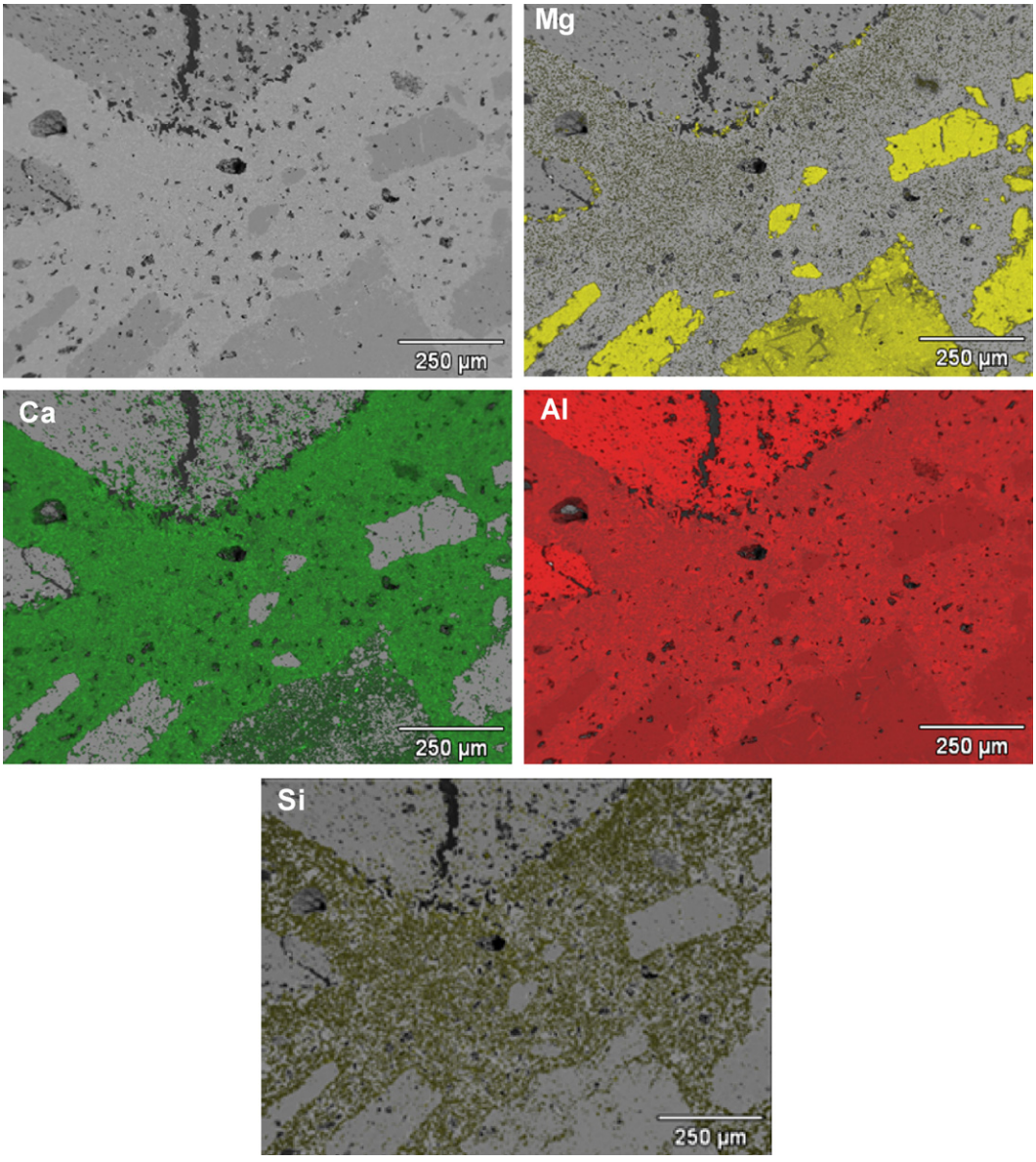

Fig. 9. Chemical mapping indicating the distribution of magnesium (Mg), calcium (Ca), aluminum (Al) and silicon (Si) in a representative area of zone (ii).

Table 4
Liquid composition of all corroded regions (from zone (ii) to zone (iv)) and also local bulk compositions in the slag zone (v).

Oxides	Content (wt%)						
	Zone (ii)	Zone (iii)	Zone (iv)	Zone (v)			
Na_2O	5.94	2.83	2.15	0.44	0.18	0.00	0.00
MgO	2.63	1.95	2.48	0.09	2.27	0.12	6.29
Al_2O_3	33.12	28.24	27.61	50.42	8.18	40.00	58.98
SiO_2	35.22	36.11	38.47	4.62	0.97	18.98	0.09
CaO	21.71	25.08	24.95	35.74	3.57	37.82	0.11
MnO	0.00	1.11	0.52	2.17	15.88	0.82	11.01
FeO	0.59	2.77	2.19	6.13	68.24	1.83	23.37
P_2O_5	0.59	1.64	1.27	0.00	0.00	0.00	0.00
K_2O	0.12	0.26	0.12	0.03	0.00	0.09	0.15
TiO_2	0.02	0.00	0.16	0.36	0.70	0.34	0.00
Cr_2O_3	0.06	0.00	0.07	0.00	0.00	0.00	0.00
Sum (wt%)	100.00	99.99	99.99	100.00	99.99	100.00	100.00

the only non-quaternary component occurring in minor amounts but can be neglected.

The liquid composition in the densified layer was measured by spot EDX and comprised mainly Al_2O_3, SiO_2 and CaO. Furthermore, this densified layer had practically no FeO or MnO. Table 4 indicates the liquid composition of all corroded regions (from zone (ii) to zone (iv)) and also the local bulk compositions in the slag zone (v).

3.5. Zone (iii): thick layer (CA_6 + spinel + corundum + liquid)

The third region evaluated was completely recrystallized including all aggregates. Unlike zone (ii), where at least the corundum aggregates existed as large (poly)crystals, in this layer the aggregate shapes remained only as ghost outlines and all the phases of the assemblage were dispersed throughout both former matrix and former aggregate volumes. The recrystallization in zone (iii) was so extensive, that all phases were detected in all the locations (including spinel, CA_6, glass in the former alumina aggregates). Conversely, in zone (ii), despite the fact that the alumina aggregates were slightly glass infiltrated and had some CA_6 and other growth/overgrowth on their outlines, they essentially kept their original large crystals. Additionally, extensive presence of MnO/FeO components in glass and crystals were detected, showing a grey-darkish overall colouring, whereas in zone (ii), these compounds were absent and there was no colouring (Fig. 6b). Occasional infiltrated iron droplets were found in the cracks (Fig. 6a), which were absent in zone (ii). This layer is located roughly at a depth of 1 cm and is about 2 cm thick. This region showed the formation of a large crack and the entire zone was also crosscut by brittle cracks.

Throughout zone (iii), FeO and MnO are present, both as a solid solution within spinel, but also as minor components in the liquid phase. Fig. 10 shows a chemical map of a region in this zone. The liquid phase composition is indicated in Table 4, and is a CAS composition similar to the one from zone (ii). However, it carried a notable amount of MnO and FeO. Compared to zone (ii), the phase assemblage in zone (iii) is not different and both of them displayed densification (Fig. 9 vs. Fig. 10). Nevertheless, the amount of liquid phase in the zone (iii) matrix was higher, as pointed out by its brightness in Fig. 10.

The densified matrix of the area shown in Fig. 10 is fine grained and porosity is concentrated into larger, generally rounded bubble-like shapes, although the pore outlines are still locally angular in detail. Whereas zone (ii) (Fig. 8) was formed early in the process of recrystallizing towards a crystal-melt equilibrium texture and shows a significant fraction of crystal morphologies that still resemble or are directly taken over from the solid original castable, zone (iii) displayed the microstructure of broad equilibrium between crystals, comprising freely developed crystal habits and interstitial melt.

Fig. 11 points out the recrystallization of tabular alumina grains. These grains fully recrystallized leading to the same assemblage found in the matrix (CA_6, spinel, corundum and liquid). Alumina was blocky to angular shape like and CA_6 recrystallized into long laths. These two phases randomly grew together (without specific orientation), indicating that these are not quench crystals, but participants of an equilibrium state over an extended time. Therefore, this area is a true high-temperature crystal mass, consisting of liquid (identified in Table 4) + corundum + CA_6 + spinel (MA) at a high temperature.

Spinel crystals were also present (Fig. 12), but in a different state from the ones of the original castable (Figs. 4 and 7). In zone (iii), the original spinel grains disaggregated and were replaced by newly formed spinel spread throughout the matrix. At this point, FeO and MnO entered the spinel phase in solid solution, surrounded by a liquid. Spot EDX of these spinel grains indicated amounts of roughly 10.0 wt% of FeO and 2.5 wt% of MnO.

Additionally, this region is also characterized by cracks (Fig. 6), which are in general brittle open fractures. Fig. 13 shows a chemical mapping of a cracked area within zone (iii). The map shows that besides the latest, through-going brittle cracks, there are also veins that comprise mostly (Mn–Fe) spinels. These veins may be derived from earlier brittle fracture sets, but now include various dense infilling with spinel plus a certain extent

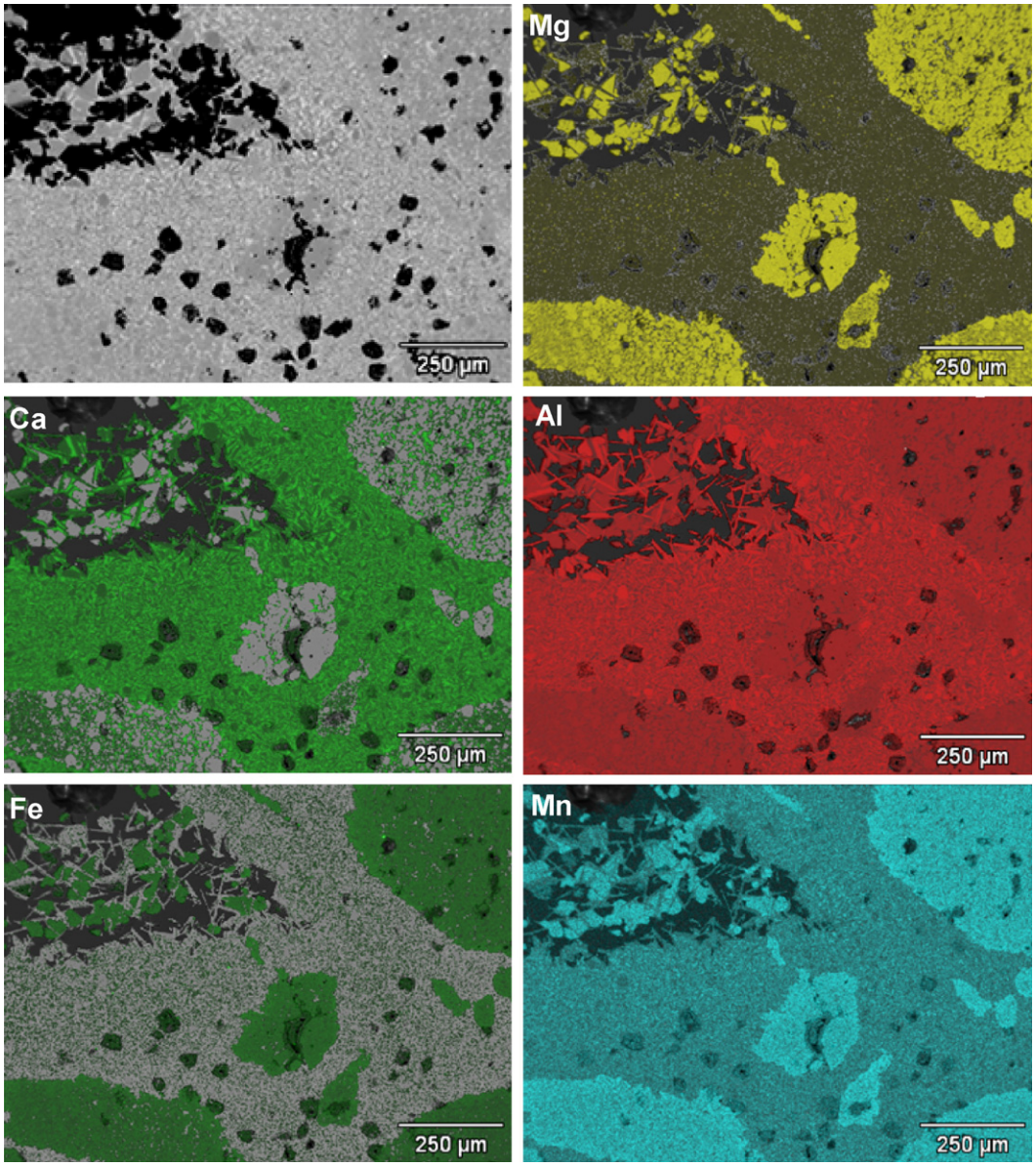

Fig. 10. Chemical mapping indicating the distribution of magnesium (Mg), calcium (Ca)–which also indicates silicon (Si) location as both were combined in the liquid phase, aluminum (Al), iron (Fe) and manganese (Mn) in a representative area of zone (iii).

of backreaction into the walls. Conversely, the Fe ion distribution indicates that the latest brittle cracks (with Fe liquid infill) do sometimes (re)use the earlier veins, but not always. In addition, Fig. 13 area shows the border between a ghost alumina aggregate (Al ion distribution) and matrix, pointing out that the vein (earlier crack, infilled) also goes through the matrix (as indicates Mg and Ca ion distributions).

3.6. Zone (iv): extended wearing region

According to Fig. 6, in zone (iii) the alumina aggregate shapes (ghosts) are still clearly visible. Nevertheless, in zone (iv), the ghost-aggregates appear to become fragmented and "dissolve" into smaller pieces, as if they become scattered through the matrix. This loss of coherence of aggregate ghosts implies a significantly stronger degree of "reworking" of the material, which means that all the alumina does not stay in one place anymore. Therefore, all the crystallites of the newly recrystallized crystal mass seem to become actively mixed and mingled through each other, so that the original aggregate-matrix distinction disappears.

Considering these aspects, it could have turned out that also a phase composition change took place. However, the results indicated that the phase compositions remained constant over all the zones, including zone (iv). In Fig. 14, the chemical mapping shows calcium hexaluminate platelets and (Mn–Fe) spinel grains at the edge of a dissolved tabular alumina grain, suggesting indirect grain dissolution. Nevertheless, as these formed layers were incomplete, a direct attack of slag via pores and grain boundaries took place, as suggested previously by the

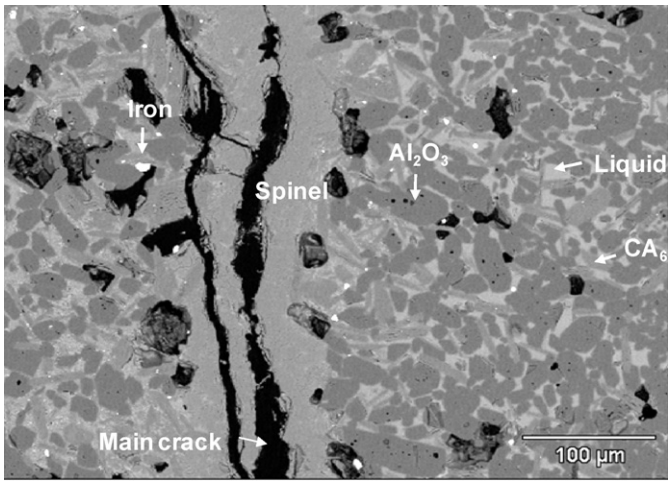

Fig. 11. Tabular alumina grain recrystallization in zone (iii), leading to a high-temperature crystal mush with liquid + Al_2O_3 + CA_6 + spinel assemblage.

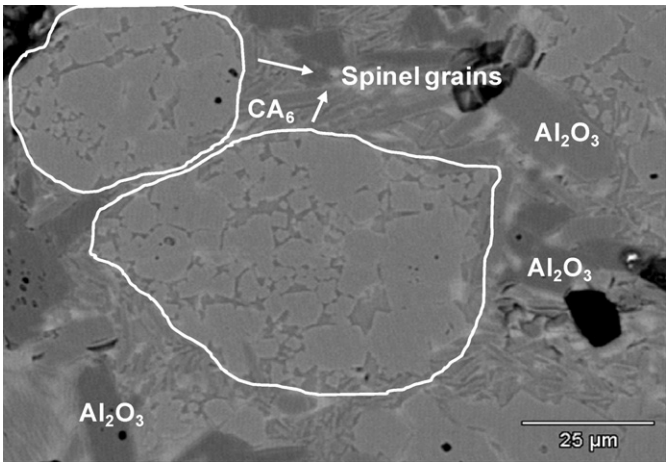

Fig. 12. Spinel grain recrystallization in zone (iii).

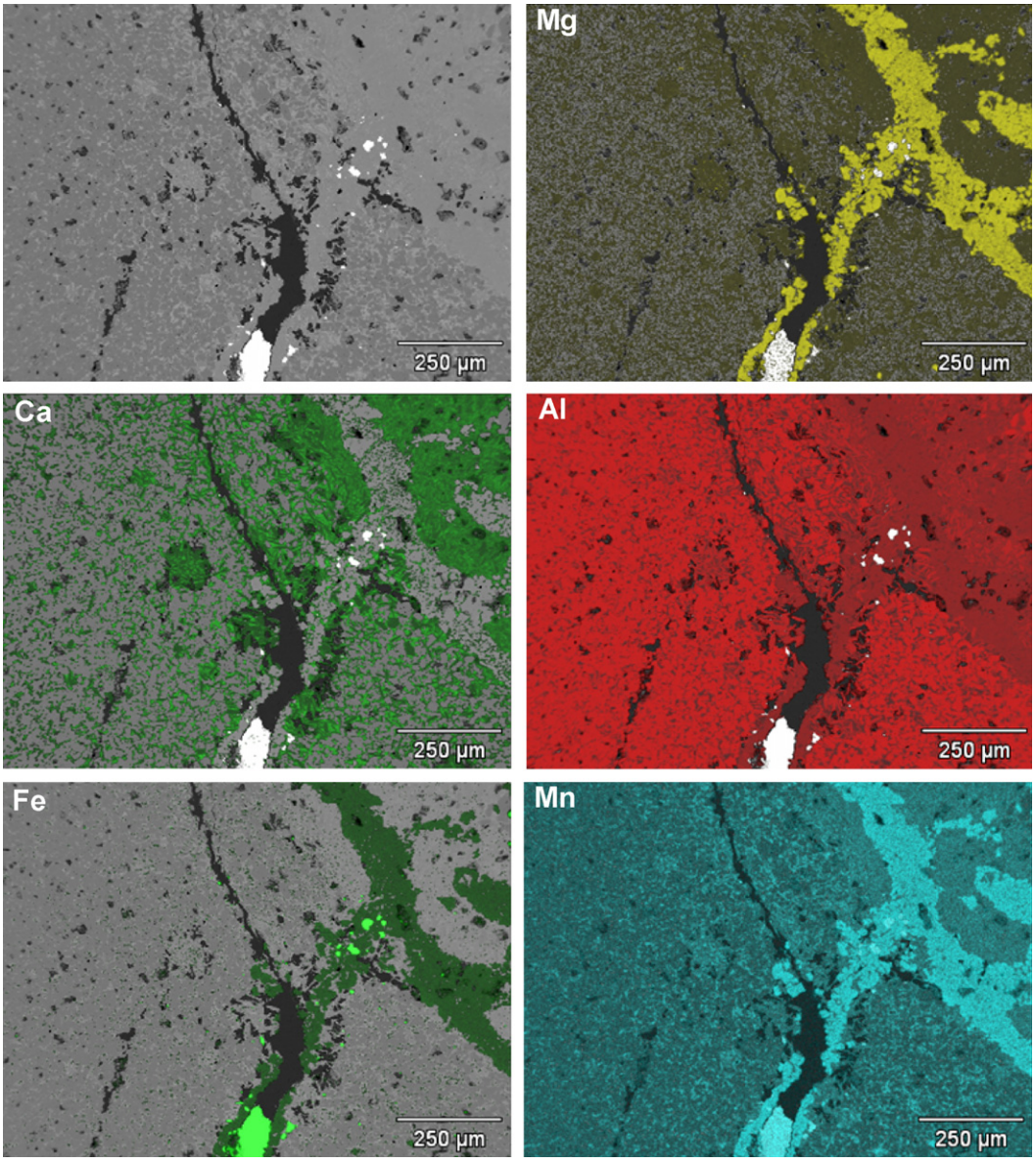

Fig. 13. Chemical mapping indicating the distribution of magnesium (Mg), calcium (Ca), aluminum (Al), iron (Fe) and manganese (Mn) in a cracked area within zone (iii).

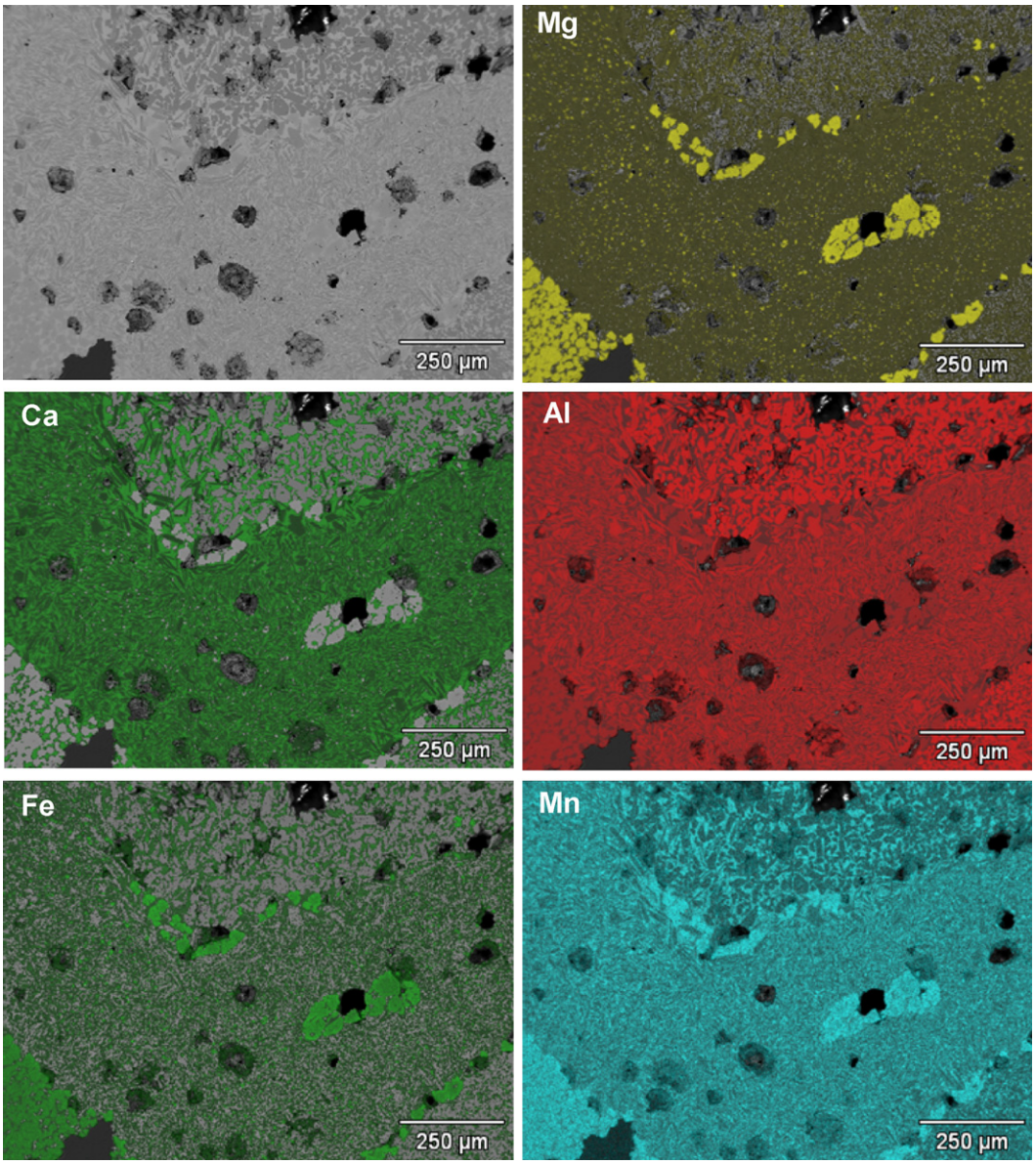

Fig. 14. Chemical mapping indicating the distribution of magnesium (Mg), calcium (Ca), aluminum (Al), iron (Fe) and manganese (Mn) in a representative area of zone (iv).

literature [7]. The matrix of this region comprised CA_6 and mainly a high amount of FeO–MnO–CAS liquid. Although the amount of liquid is higher compared to the other zones, its composition is nearly the same as in zone (iii) (Table 4).

3.7. Zone (v): top layer (recrystallized liquid + CA_6 + spinel)

Zone (v) is a thin layer (<5 mm) capping the outermost surface of the well block wear profile and its outside is exposed to the operating volume of the ladle. In this zone, a variation of different slags is detected, which were partially crystalline at the high temperature stage. This slag was also completely crystallized when it was last cooled into relatively finer grained quenched phases. Fig. 15 presents a chemical map of an area in this zone and shows that at the top the slag are oxidic slag liquids, fully quench crystallized and with lower silica content than those observed in the previous zones. Phase assemblages vary in the variable slag, but are mostly characterized by spinel and CA_6 as high temperature stable phases. Local bulk area compositions (representative area EDX scans), approximating the bulk slag compositions at high temperatures, are given in Table 4. These compositions show a marked reduction of the silica content in this layer. The bright white drops are metallic iron, however the compositions also show that a substantial amount of the iron present is incorporated in oxidized form in the slag. The same increased degree of oxidation is also indicated by the appearance of a calcium ferrite phase among the quench phase (low Al, low Si, high Ca areas in Fig. 15; middle grey in the BSE image). At the outermost surface, strong oxidation, most likely due to interaction with an oxygen-rich atmosphere during cooling, is shown by the appearance of

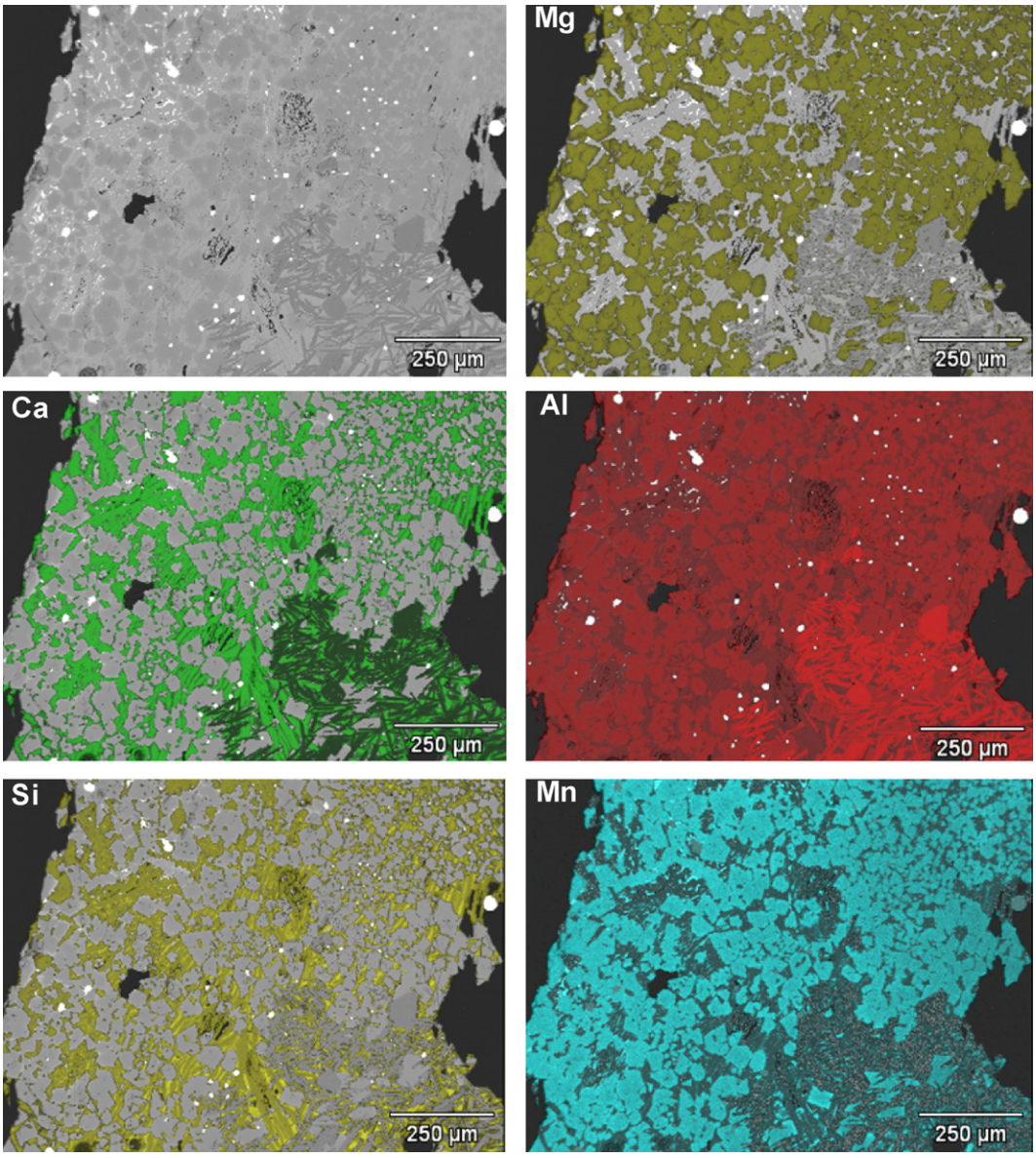

Fig. 15. Chemical mapping indicating the distribution of magnesium (Mg), calcium (Ca), aluminum (Al), silicon (Si) and manganese (Mn) in a representative area of zone (v).

ferritic spinels in overgrowth rims on the quench phases (thin interstitial rims in the upper left corner of Fig. 15).

4. Discussion

The initial stage of chemical attack, visible in the deepest preserved reaction zone, took place in the densified layer (zone (ii)). As the castable evaluated in zone (i) behaved similarly to the experimental one fired at 1500 °C (Fig. 4b compared to Fig. 7), the original well block refractory attained high temperatures at this depth (zone (i), >5 cm), but was not fully affected by penetration and corrosion. Therefore, the main reason for the formation of a sharp front to the densified layer in zone (ii) was not the thermal freezing of the infiltrating liquid, but a consequence of attaining an equilibrium state with increased liquid viscosity and due to the capillary force balance. According to Korgul et al. [24] and Nagai et al. [25], calcia from the slag reacts with alumina in the refractory, leading to the precipitation of calcium aluminates such as CA_2 and CA_6. In deeper areas of the refractory, as alumina and lime were previously consumed, the relative amount of silica increases, generating a high viscosity and high melting temperature local slag, which then hinders further slag penetration. In this study, although CA_6 was detected, CA_2 was not, which must be a consequence of a high SiO_2 content in the infiltrated and reacted liquid.

The change of chemical composition of the matrix as observed in zone (ii) can be used to constrain the extent and nature of the reaction with an external reactant using a mass balance modeling, which can provide an idea of the amount and composition of the infiltrated liquid. The composition of the densified layer, C_i^{DL}, is the result of the reaction between the

original matrix with its composition, C_i^{OM} and an external reactant, C_i^{ER}. The extent of reaction can be traced by an interaction parameter "a", where the unit mass of product matrix is formed by $0 < a < 1$ of the original matrix plus $(1-a)$ of the reactant addition. Element exchange (i.e. loss of an element to an external reservoir) is accommodated by allowing the compositional vector elements in C_i^{ER} to be negative. For each element i, a mass balance equation can be written as follows:

$$a \times C_i^{OM} + (1-a) \times C_i^{ER} - C_i^{DL} = 0 \quad (1)$$

This equation together with the closure constraint in each composition, $\sum_i C_i = 1$, yields a unique solution for the interaction, quantifying both the chemical composition C_i^{ER} of an external reactant and the amount of reaction required to explain the observed chemical change in the matrix. However, the exact solution of this system of linear equations can be strongly dependent on errors in determining original and changed matrix compositions. Therefore, an exact solution may be a fluctuation satisfying measurement errors instead of reality. Due to this reason, a more suitable way to treat the reaction is to analyze the behavior of the output variable as one varies the interaction between its bounds (from 0 to 1).

Considering the matrix chemical composition of zone (i) and zone (ii) (Table 3), the composition of the external reactant of each oxide (SiO_2, Al_2O_3, MgO and CaO) can be calculated as a function of the mass fraction of the external reactant in the product matrix (Fig. 16). Assuming zero Al (and, therefore, no alumina) in the infiltrant and no net Al release out of the reaction zone, the possible infiltrating slag composition, which resulted in zone (ii) matrix from the original castable, can be derived. From the $CaO–Al_2O_3–SiO_2$ equilibrium phase diagram (Fig. 17) [26], the original matrix composition of zone (i) can be located (spot A, from Table 3) as well as the CaO/SiO_2 ratio of the infiltrating liquid (spot B, from Fig. 16, considering $Al_2O_3 = 0$, a ~0.8 and, thus, CaO ~35 mass% and SiO_2 ~65 mass%). The arrow that links both spots is the chemical change vector and the highlighted box underscores the possible solid saturated liquid compositions at temperatures ranging from 1400 to 1500 °C. As no anorthite (CAS_2) was observed, the matrix is instead saturated with a slag having a compositions within the CA_6 primary liquidus field and thus the infiltrating liquid cannot be more SiO_2 rich than the 1495 °C peritetic CA_6-out reaction point, which is about 35 vol% of SiO_2.

This aspect supports the apparent flatness of the thermal profile in the well block and brings to the discussion the problem of where such a liquid could come from, as the ladle slag is generally a calcium aluminate source with at most a few percent of silica (Table 1). One of the alternatives, due to the location, is the well block filler sand, which comprises mainly chromium and silica. Although it is a clear silica source, chromium was not detected by the EDX analyses. Additionally, the wear mechanism of a steel ladle alumina-spinel castable explained by Nagai et al. [25] points out that penetration is suppressed in this system due to the rise in the melting point and viscosity of the slag (high silicon), after alumina and spinel from the castable capture CaO, FeO and MnO from the slag.

Based on the infiltrating liquid composition (about 32–36 wt% SiO_2), its content would be close to 40 vol% (Fig. 16). Plotting the composition of the matrix of zone (ii) (Table 3, spot C, Fig. 17) underscores the need of a substantial amount of infiltrating liquid in order to change the composition from the original (spot A) to the one detected in the densified layer (spot C). Considering that the original matrix porosity estimate was up to 36 vol% and the porosity estimate of the matrix of zone (ii) was 9–10 vol%, only some 26 vol% of an external liquid can have been stored without bulk volume change. As a consequence, to accommodate enough of a calcium alumino-silicate liquid to create zone (ii) from zone (i), the local well block must either have expanded (volume growth) and/or

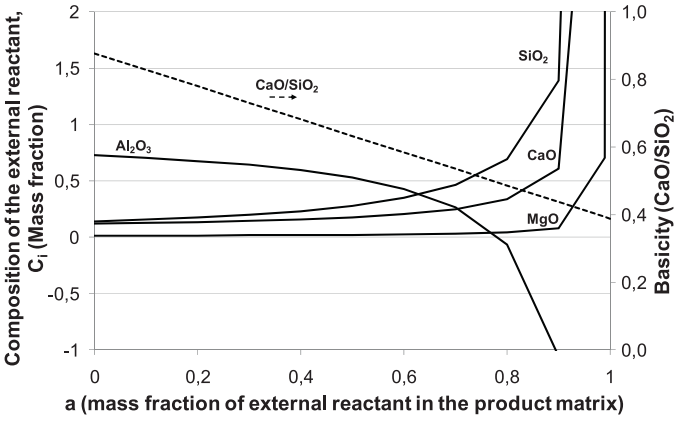

Fig. 16. Composition of the external reactant for each oxide (SiO_2, Al_2O_3, MgO and CaO) as a function of the mass fraction of the external reactant in the product matrix (a).

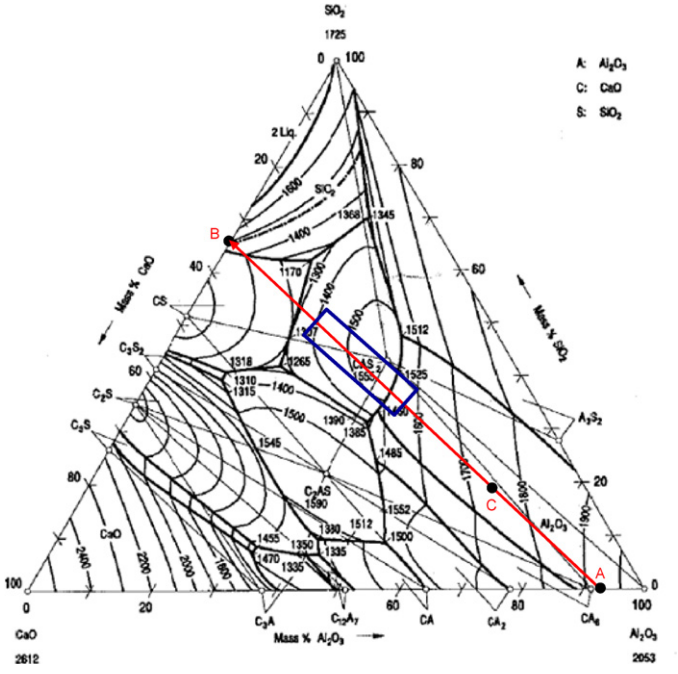

Fig. 17. $CaO–Al_2O_3–SiO_2$ equilibrium phase diagram [26]. Spot A and C came from Table 3, whereas spot B was calculated from Fig. 16 (assuming Al = 0).

significant quantities of mostly Al_2O_3 must have leached out. A net growth corresponds with the cracks that are locally observed throughout the densified layer (Fig. 9) in alumina aggregate grains and that tend to terminate against the matrix.

Zone (iii) also contains a system of cracks, the formation of which can be understood considering the chemical maps shown in Fig. 13. In this figure, veins containing MnO/FeO-rich spinel and liquid iron are detected. However, as metallic iron droplets are distributed over both the infilled veins and the brittle cracks, different cracking episodes took place in this region at different periods of time, with the brittle cracking as a separate and later generation of fracturing. Spinel lining formed on the earlier vein generation and is a product of infilling cracks (pathways) from a crystallizing infiltrating melt. Where the later, brittle cracks do not reuse earlier veins, they also do not have spinel sidewalls, pointing out that spinel formation did not occur in connection with the later cracks. As these later cracks still were Fe liquid pathways, the formation of this system of cracks must have been related to the thermal up-shock caused by the filling of the ladle with steel.

This aspect is consistent with the cyclic character of the ladle operation, where in the cooling off stage in between ladle heats, the well block upper level, which was turned into a crystal mass bound by a silicate liquid during the hot part of the process, cools to glassify and this makes it sensitive to thermal shock. Then, tapping hot steel onto it in the next cycle, this region is subjected to up-shocks, leading to fracture, and Fe liquid infiltrates before remelting the zone, while conditions stay properly reduced below Fe/FeO. After thorough reheat and partial remelting of the crystal mush zone, reactions between the infiltrating metal (plus–minus ladle glaze) creates spinel veins, which are not purely brittle anymore in their appearance, but infiltration-reaction veins. These cool off together with their surroundings in the next cycle and the reaction product of the refractory after extended service is more sensitive to thermal shock than the original refractory. Considering this, extended chemical corrosion can lead to failure due to thermal shock. Consequently, corrosion generates the infiltration of a glassy phase that can result in thermal shock sensitivity, whereas thermal shock can generate cracks that can assist further penetration.

Another characteristic of the process cycle of the steel ladle is associated with the variable iron oxidation states (metallic or oxidic) observed in the well block sample. The process cycle consists of two parts: one at high temperatures when the steel is in contact with the top of the well block, generating the situation stated above, and another at low temperatures when ladle glaze and remains of ladle slag are in contact with the well block. Only at this later step, the conditions on the top of the well block oxidize enough to allow significant FeO and MnO contents in the infiltrating slag. Thus, zone (iii) which shows the formation of FeO/MnO-containing spinel, has interacted with liquids from a different process cycle segment than zone (ii) (densified layer), which was only corroded by a CAS slag.

According to the literature [3], the more rapidly diffusing species such as Fe and Mn are preferentially taken up by spinel and then a high silica containing slag would be formed limiting further penetration and corrosion. This silica enrichment in the slag concurs with the formation of the densified layer (zone (ii)), as the melt is then more viscous than the one containing Fe, Mn and Ca. Nagai et al. [25] proposed, after testing a alumina-spinel castable by rotary slag corrosion, a mechanism to explain the corrosion of this system by basic slag which indicates that CaO, FeO and MnO from the slag are firstly captured by alumina (generating CA_6) and spinel (forming MnO–FeO spinel). Due to this reason, the composition of the slag changes (CAS, high silicon) and its viscosity is increased, suppressing further penetration. This experimental result is in accordance with the well block *post mortem* analyses (Fig. 18), validating laboratory tests in order to attain the most suitable corrosion resistant refractory castable for steel ladle application.

At the low temperature oxidized part of the process, the well block is covered by the ladle slag, which is then rich in FeO and MnO. This new liquid is laid on the top of the well block, which already contains another liquid infiltrated to a depth of a few centimeters. Considering this, the new liquid does not need to penetrate, as the porosity below was already widely liquid

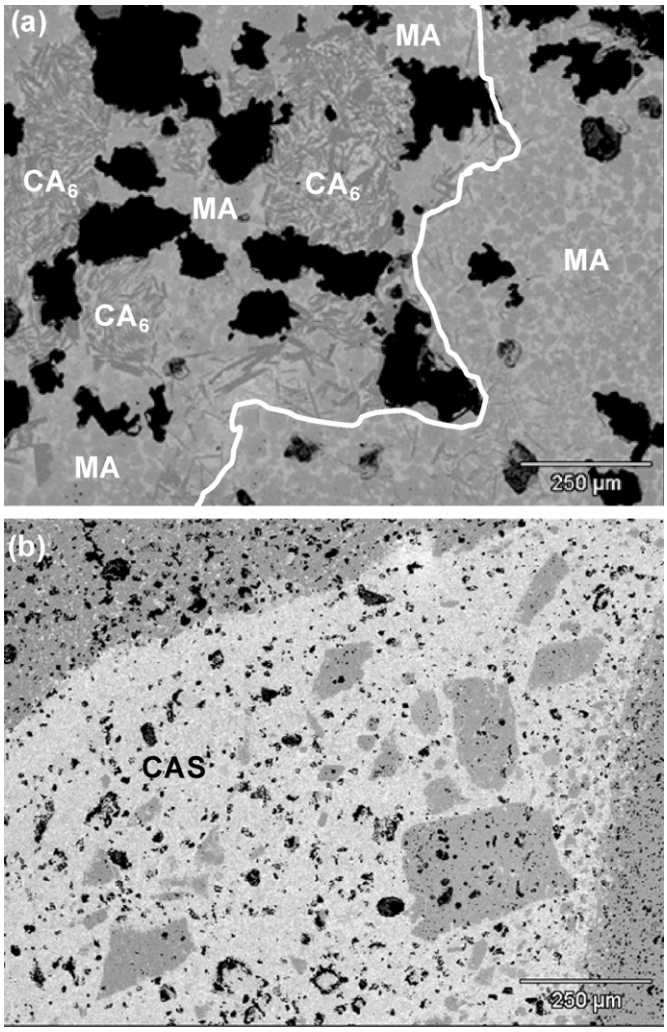

Fig. 18. Agreement between laboratory tests from the literature [3,25] and the well block practical observations: (a) zone (iii) to zone (iv)–extensive CA_6 and MnO/FeO spinel (MA) formation; (b) zone (ii)–CAS liquid (high silicon).

infiltrated. Instead, the two liquids mix, driven by an advection process. The efficiency of the mixing process is seen in the lack of a significant compositional (diffusion) gradient in either spinel or liquid compositions observed from the top of the well block sample down to zone (iii). The uniformity of the phase assemblage and compositions throughout the top zone indicates that advection (fluid's bulk motion in a particular direction) rather than diffusion was the main mixing process of the two liquids and, consistently, the mixing is locally very heterogeneous. This aspect can be evaluated by the different shades of blackness of the local well block top zones (iii) and (iv) (Figs. 2 and 6b).

In consequence, this partially molten well block top layer can take up FeO/MnO and store it during the oxidized part of the ladle cycle and give it off again to the steel in the reduced part, which effectively releases oxygen into the steel. Due to this feature, the chemically altered well block presents a reoxidation potential to the steel. Therefore, unwanted inclusions can be created at a critical position in the ladle, in the worst case even increasing the risk of clogging. Due to its location, if the well block manages to contaminate the steel around it and to induce, for instance, ladle clog from inclusions, the process and steel quality would deteriorate, regardless of the steel treatment carried out in the ladle above it.

In addition, the assemblage of zone (iii) is relatively erodible due to it being liquid bonded, but could not be immediately washed away, due to the high content of solids (roughly 90–95 vol%), leading to a high bulk viscosity. If this upper part erodes/disggregates, it can give off material into steel directly in the vicinity of the ladle nozzle. This erosion most likely takes place when the ladle is emptied, meaning that just at the most sensitive step of the steel making process (casting), the steel can be seeded with fragments of eroded well block, spoiling the cleanliness of the steel.

5. Conclusions

The *post mortem* well block evaluation highlighted the following aspects:

(i) An intense slag liquid infiltration can result in expansion, which will always induce a risk of fracture
(ii) As infiltration takes place, the glassy phase would be present at the cooling stage of the steel ladle process and, during its cooling or heating up, there will be more likelihood for down or up thermal shock. This would lead to further crack formation and infiltration and continuous damage to the refractory material
(iii) As a consequence of the partially molten structure close to the area in contact with steel, erosion could take place and result in unwanted inclusions, which could spoil the steel quality just after its treatment in the ladle.

Considering these aspects, the reduced refractory castable consumption is due to corrosion (in order to attain the equilibrium state, highlighted by the formation of the densified layer), the more protected the original material will be in terms of thermal shock, corrosion and erosion. To reduce the formation (and size) of the detected layers, higher contents of alumina should be added to the castable composition, in order to pick up greater amounts of CaO and Al_2O_3 from slag, increasing its local silica content (and viscosity) and inhibiting further penetration. In this sense, the reduction in the CaO content is a key aspect, in order to keep any equilibrium liquid in the infiltration as long as possible in the alumina liquidus field, as that has the highest SiO_2 contents and hence the most difficult internal mobility. Following these suggestions, an extended working life and clean steel production could be attained.

Acknowledgments

The authors are grateful to the Federation for International Refractory Research and Education (FIRE) and the Brazilian Research Funding FAPESP for supporting this work. Furthermore, the authors are thankful to Warbout Tesselaar, Christian Liebske, Frank van der Does and Max Koolwijk from the Corus Ceramic Research Centre for the well block sampling and SEM spectral imaging.

References

[1] E. Blond, N. Schmitt, F. Hild, P. Blumenfeld, J. Poirier, Thermomechanical stresses in slag-impregnated refractories, in: In Proceedings of Unified International Technical Conference on Refractories 2001, The American Ceramic Society (USA), Cancun, Mexico, 2001, pp. 1340–1348.
[2] R.A. Mattila, J.P. Vatanen, J.J. Härkki, Chemical wearing mechanism of refractory materials in a steel ladle slag line, Scand. J. Metall. 31 (2002) 241–245.
[3] W.E. Lee, S. Zhang, Melt corrosion of oxide and oxide-carbon refratories, Int. Mater. Rev. 44 (3) (1999) 77–104, 3.
[4] M. Chen, N. Wang, W. Liu, Preparation and properties of alumina–magnesia precast block for ladle lining, Mater. Lett. 61 (2007) 3388–3390.
[5] H. Hattanda, A. Kato, S. Morimoto, Advanced precast blocks, Taik. Overs. 19 (3) (1999) 39–43.
[6] H. Sarpoolaky, S. Zhang, B.B. Argent, W.E. Lee, Influence of grain phase on slag corrosion of low-cement castable refractories, J. Am. Ceram. Soc. 84 (2) (2001) 426–434.
[7] S. Zhang, H.R. Rezaie, H. Sarpoolaky, W.E. Lee, Alumina dissolution into silicate slag, J. Am. Ceram. Soc. 83 (4) (2000) 897–903.
[8] B.A. Vázquez, P. Pena, A.H. de Aza, M.A. Sainz, A. Caballero, Corrosion mechanism of polycrystalline corundum and calcium hexaluminate by calcium silicate slags, J. Eur. Ceram. Soc. 29 (2009) 1347–1360.
[9] H. Sarpoolaky, S. Zhang, W.E. Lee, Corrosion of high alumina and near stoichiometric spinels in iron-containing silicate slags, J. Eur. Ceram. Soc. 23 (2003) 293–300.
[10] M.A.L. Braulio, D.H. Milanez, E.Y. Sako, L.R.M. Bittencourt, V.C. Pandolfelli, Expansion behavior of cement bonded alumina–magnesia refractory castables, Am. Ceram. Soc. Bull. 86 (12) (2007) 9201–9206.
[11] L.A. Díaz, R. Torrecillas, A.H. de Aza, P. Pena, Effect of spinel content on slag attack resistance of high alumina refractory castables, J. Eur. Ceram. Soc. 27 (6) (2007) 4623–4631.
[12] S. Zhang, W.E. Lee, Spinel-containing refractories, in: C.A. Schacht (Ed.), Refractories Handbook, Marcel Dekker, Inc., New York, NY, 2004, pp. 215–257.
[13] V. Bhatnagar, S. Mukhopadhyay, C. Natarajan, Development of improved quality spinel castable for steel ladle bottom, in: UNITECR'05, Proceedings of Unified International Technical Conference on Refractories, Orlando, USA, (2005), pp. 162–166.

[14] A. Molin, J. Molin, J. Podworny, T. Wala, Corrosion mechanism of spinel forming and spinel containing refractory castables in lab an plan conditions, in: UNITECR'05, Proceedings of Unified International Technical Conference on Refractories, Orlando, USA, (2005), pp. 57–62.
[15] K. Goto, B.B. Argent, W.E. Lee, Corrosion of MgO–$MgAl_0O_4$ spinel refractory bricks by calcium aluminosilicate slag, J. Am. Ceram. Soc. 80 (2) (1997) 461–471.
[16] M.A.L. Braulio, J. Poirier, L.R.M. Bittencourt, V.C. Pandolfelli, Microsilica effects on cement bonded alumina–magnesia refractory castables, J. Technol. Assoc. Refract–Japan 28 (3) (2008) 180–184.
[17] E.Y. Sako, M.A.L. Braulio, D.H. Milanez, P.O. Brant, V.C. Pandolfelli, Microsilica role in the CA_6 formation in cement-bonded spinel refractory castables, J. Mater. Process. Technol. 209 (2009) 5552–5557.
[18] J.M. Auvray, C. Gault, M. Huger, Microstructural changes and evolutions of elastic properties versus temperature of alumina and alumina–magnesia refractory castables, J. Eur. Ceram. Soc. 28 (2008) 1953–1960.
[19] W.E. Lee, W. Vieira, S. Zhang, A. Ghanbari, H. Sarpoolaky, C. Parr, Castable refractory concretes, Int. Mater. Rev. 46 (3) (2001) 145–167.
[20] J. Mori, Structure change of alumina castable by addition of magnesia or spinel, Taik. Overs. 15 (3) (1995) 20–23.
[21] M. Kobayashi, K. Kataoka, Y. Sakamoto, I. Kifune, Use of alumina–magnesia castables in the steel ladle sidewall, Taik. Overs. 17 (3) (1997) 39–44.
[22] M. Nanba, T. Kaneshage, Y. Hamazaki, H. Nishio, I. Ebizavawa, Thermal characteristics of castables for teeming ladle, Taik. Overs. 16 (3) (1997) 17–21.
[23] N. Shirama, K. Murakami, I. Shimizu, Development of low silica wet gunning material for steel ladles, J. Technol. Assoc. Refract–Japan 22 (2) (2002) 161–163.
[24] P. Korgul, D.R. Wilson, W.E. Lee, Microstructural analysis of corroded alumina-spinel castable refractories, J. Eur. Ceram. Soc. 17 (1) (1997) 77–84.
[25] N. Nagai, O. Matsumoto, T. Isobe, Y. Nishimi, Wear mechanism of castable for steel ladle by slag, Taik. Overs. 12 (1) (1992) 15–20.
[26] Al_2O_3–CaO–SiO_2, Slag Atlas, 2nd edition, Verein Deutscher Eisenhüttenleute (VDEh), Verlag Stahleisen GmbH, Germany, 1995, p. 105.